Polymer Chemistry

Accepted Manuscript

This article can be cited before page numbers have been issued, to do this please use: E. Tinajero Diaz, E. C. Zamora and A. Martínez de Ilarduya, *Polym. Chem.*, 2025, DOI: 10.1039/D5PY00594A.

ROYAL SOCIETY OF CHEMISTRY

rsc.li/polymers

View Article Online
DOI: 10.1039/D5PY00594A

ARTICLE

Bio-based poly(1,3-trimethyleneglycol-*co*-lactide) triblock copolymers: a promising platform for biomedical applications

Ernesto Tinajero Díaz,[‡a] Eduard Carles Zamora[‡a] and Antxon Martínez de Ilarduya*[a]

Received 00th January 20xx,
Accepted 00th January 20xx

DOI: 10.1039/x0xx00000x

A series of bio-based poly(lactide)-*b*-poly(1,3-trimethylene glycol)-*b*-poly(lactide) copolymers covering the whole range of compositions was synthesized by ring-opening polymerization (ROP) of *L*- or *D,L*-lactide initiated by bio-based poly(1,3-trimethylene glycol). The copolymers were obtiained by bulk polymerizations carried out at 180 °C, using stannous octoate as the catalyst. The triblock structure was confirmed by both ^{1}H NMR and SEC analyses. It was observed that molecular weights increased while dispersities decreased with the increasing content of lactide units in the copolymer. Copolymers prepared with *L*-lactide exhibited crystallinity with melting points and enthalpies increasing with the length of lactide blocks in the copolymers. In contrast, copolymers based on *rac*-lactide were fully amorphous, regardless of composition. All copolymers displayed a single glass transition temperature (T_g), which increased *quasi*-linearly with increased lactide content, indicating good miscibility betwen polyether and polyester blocks. Furthermore, they demostrated thermal stability up to aproximatelly 250 °C, and exhibited a two-step decomposition process, corresponding to the degradation of polyester and polyether segments. Finaly, the amphiphilic nature of these copolymers was confirmed, as all of them were capable to self-assemble in water, forming spherical nanoparticles with ζ-average diameters ranging from 95 to 158 nm.

Introduction

In the global transition to achieve a sustainable and circular economy, the introduction of innovative materials for packaging and biomedical applications from bioresource stocks is highly appreciated.[1-3] Poly(trimethylene glycol) ($PO3G_n$), for instance, is a fully bio-based polyether obtained by condensation of 1,3-propanediol (PDO), which is directly produced from a fermentation glucose proccess.[4, 5] Interestingly, the chemical structure of $PO3G_n$ resembles to that of poly(ethylene glycol) (PEG) with one additional methylene in the repeating unit. Typical molecular weights range from approximately 250 to 2,700 g·mol^{-1} and dispersities between 1.5 and 2.0.[6] Thus, the polyol can serve as a promising alternative to design novel polymer architectures. It has been used for the synthesis of renewable elastomeric thermoplastics polyesters,[7] polyamides[8] and polyurethanes.[6, 9-12] On the other hand, in the biomedical field, the use of PEG in various pharmaceutical formulations, including cosmetics and soaps, among others, has been shown to induce the formation of anti-PEG antibodies, which can reduce the efficacy of PEGylated drugs.[13, 14] Therefore, its replacement with PO_3G_n for the different formulations could represent a promising alternative approach, although a lower degree of hydrophilicity can be expected. This polyol exhibits both lower critical solution temperature (LCST) and upper critical solution temperature (UCST) in a range of temperatures between 30-80 °C, which can be used for the preparation of thermosensitive nanomaterials.[5, 15]

Poly(lactic acid) (PLA) is another interesting bio-based, biodegradable and biocompatible aliphatic polymer, obtained by ring-opening polymerization (ROP) of lactide (cyclic dimer of lactic acid).[16-18] The crystallinity of this polyester can be tuned by the enantiomeric composition of lactides used in the feed.[19, 20] This polyester finds applications in the fields of packaging[21, 22] and biomedicine.[16, 23]

The integration of PO_3G_n and PLA presents a versatile platform for the development of fully biobased polymers with finely tunable properties. Owing to the presence of two terminal hydroxyl groups, PO_3G_n can act as an efficient macroinitiator for the ROP of lactide, leading to the formation of amphiphilic copolymers capable of self-assembling in aqueous environments.

This paper describes a protocol for the synthesis and characterization of poly(lactide-*b*-polytrimethylene glycol-*b*-lactide) triblock copolymers, abbreviated as PLA_m-*b*-$PO3G_n$-*b*-PLA_m, through bulk ROP of either *L*- or *rac*-lactide covering a wide range of compositions. The polymerization was initiated by $PO3G_n$ macroinitiators of three different molecular weights ranging from 500 g·mol^{-1} to 2,400 g·mol^{-1}. For each macroinitiator three different triblock copolymers containing either *L*-lactide or *rac*-lactide were produced varying the $PO3G_n$/lactide molar feed ratio. By precisely controlling the copolymer architecture, including composition, stereochemistry, and molecular weight, it was possible to modulate key material attributes such as thermal properties

[a] Department d'Enginyeria Química, Universitat Politècnica de Catalunya, ETSEIB, Diagonal 647, 8028 Barcelona, Spain. E-mail: antxon.martinez.de.ilarduia@upc.edu
‡ These authors contributed equally.
† Supplementary Information available: See DOI: 10.1039/x0xx00000x

and stability. Finally, and as a proof-of-concept, we explored the ability of these copolymers to self-assemble in water using the emulsion/solvent-evaporation method. The biomedical field demands an expansion of available materials for drug delivery, especially for addressing challenges for an efficient delivery of therapeutic agents to the target site. $PO3G_n$, for example, can be an eco-friendly alternative to PEG, the gold-standard polymer used in drug delivery due to its 'stealth' properties, although already mentioned, it has proven to be less immunologically inert than originally anticipated. [24, 25]

This strategy paves the way for the design of high-performance, sustainable materials tailored to meet the requirements of advanced technological and biomedical applications.

Experimental

Materials

Poly(trimethylene glycol) ($PO3G_n$, MW=500 g·mol^{-1}, 1,000 g·mol^{-1} and 2,400 g·mol^{-1}) was gifted by Allessa GmbH (Frankfurt, Germany). *L*/*rac*-lactide (>99.0%) was donated by Corbion (Amsterdam, The Netherlands) and was stored in silica gel and vacuum at -10 °C prior to use. Tin-2-ethylhexanoate ($Sn(Oct)_2$ 92.5-100%) was acquired from Sigma Aldrich and used as received. Poly(vinyl alcohol) (PVA, M_W=3000 g·mol^{-1}, 88% hydrolysed) was obtained from Scientific Polymer Products. Solvents, chloroform ($CHCl_3$, ≥99.8%) and dichloromethane (DCM, ≥99.8%), were used as received.

General methods

^{1}H and ^{13}C NMR spectra were recorded on a Bruker AMX-300 spectrometer at 25 °C, operating at 300.1 and 75.5 MHz, respectively. Compounds were dissolved in deuterated chloroform ($CDCl_3$) and spectra were internally referenced to tetramethylsilane (TMS). About 10 and 50 mg of sample in 1 mL of solvent were used for ^{1}H and ^{13}C NMR, respectively. Sixty-four scans were recorded for ^{1}H, and between 5,000 and 20,000 for ^{13}C NMR.

Size exclusion chromatography (SEC). Molecular weights were determined using chloroform as eluent in a Waters equipment (Foster City, CA, USA), provided with RI and UV detectors and HR5E and HR2 Waters linear Styragel columns (7.8 mm × 300 mm). Of the sample solution, 0.1 mL (0.1% w/v) was injected and chromatographed with a flow rate of 0.5 mL·min^{-1}. The molar mass averages and distributions were calibrated against PMMA standards.

Fourier transform infrared spectra (FT-IR) were acquired using a Perkin-Elmer Frontier FT-IR spectrometer (Waltham, MA, USA), provided with a universal-attenuated total reflectance (ATR) accessory. Infrared spectra were recorded in the 4,000-650 cm^{-1} range at a resolution of 4 cm^{-1}, and 16 scans were collected.

The thermal behaviour of polymers was examined by differential scanning calorimetry (DSC) using a Perkin-Elmer DSC 8000 apparatus. The thermograms were obtained from 4-6 mg samples at heating and cooling rates of 10 °C·min^{-1} under a nitrogen flow of 20 mL·min^{-1}. Indium and zinc were used as standards for temperature and enthalpy calibration. The glass transition temperature (T_g) was extracted from the inflection point of the heating traces recorded at 20 °C·min^{-1} from melt-quenched samples, and the melting temperature was taken as the maximum of the endothermic peak arising on the heating traces recorded from samples crystallized from the melt.

Thermogravimetric analysis (TGA) was performed on a Mettler-Toledo TGA/DSC 1 Star System under a nitrogen flow of 20 mL·min^{-1} at a heating rate of 10 °C·min^{-1} and within a temperature range of 30-600 °C.

Dynamic light scattering (DLS) measurements used for particle hydrodynamic size and ζ-potential determinations were performed with the Malvern Nano ZS instrument equipped with a 4 mW He-Ne laser operated at 632.8 nm. Particles were suspended in deionized water at 25 °C and placed in glass cuvettes. The non-invasive back-scatter optic arrangement was used in order to collect the light scattered by particles at an angle of 173°.

Scanning electron microscopy (SEM) images were taken with a field-emission JEOL JSM-7001F (JEOL, Tokyo, Japan) from platinum/palladium coated samples. Different dilutions were essayed to observe free individual nanoparticles. Images were edited using the ImageJ software.

Synthesis of PLA_m-$PO3G_n$-PLA_m triblock copolymers

Poly(*L*-lactide)$_m$-*b*-poly(trimethylene glycol)$_n$-*b*-poly(*L*-lactide)$_m$ (P*L*LA$_m$-*b*-PO3G$_n$-*b*-P*L*LA$_m$). As an example, for the synthesis of P*L*LA$_{82}$-*b*-PO3G$_{41}$-*b*-P*L*LA$_{82}$ triblock copolymer with a [PO3G]:[*L*-LA] = [1]:[4] feed molar ratio, in a 25 mL three-necked, round-bottom flask equipped with a mechanical stirrer, a nitrogen inlet and a vacuum distillation outlet, PO3G$_{41}$ (MW=2400, 0.5 g, 8.6 mmol of repeating units) and *L*-lactide (2.48 g, 17.2 mmol) were added. The flask was then immersed in an oil bath under a N_2 atmosphere for 5 min for purging the reaction system. Subsequently, the flask was heated to 120 °C and kept under vacuum for 5 additional min. Thereafter, the reaction flask was further heated to 180 °C, and polymerization began after the addition of $Sn(Oct)_2$ (1.2 mg, 3.06 μmol, 0.05% by weight relative to *L*-lactide) from a stock solution in chloroform. The reaction flask was left under stirring for ~1.5 h until *L*-lactide was fully consumed, as monitored by ^{1}H NMR. The mixture was then dissolved in DCM and precipitated into an excess of hexane. The copolymer was recovered as a white powder. Prior to characterization, the copolymer was dried at 50 °C under vacuum.

P*L*LA$_{82}$-*b*-PO3G$_{41}$-*b*-P*L*LA$_{82}$: ^{1}H NMR (300 MHz, $CDCl_3$, δ, ppm): 5.17 (q), 4.35 (q), 4.23 (m), 3.48 (t), 1.82 (qu), 1.58 (d). ^{13}C NMR (75.5 MHz, $CDCl_3$, δ, ppm): 169.5, 69.0, 67.8, 66.8, 30.1, 16.6.

P*L*LA$_m$-*b*-PO3G$_9$-*b*-P*L*LA$_m$ and P*L*LA$_m$-*b*-PO3G$_{17}$-*b*-P*L*LA$_m$ triblock copolymers. The synthesis of these copolymers was carried out in a similar fashion using the procedure described for the P*L*LA$_m$-*b*-PO3G$_{41}$-b-P*L*LA$_m$ copolymers using $PO3G_n$ macroinitiators having MW=500 and 1000 g·mol^{-1}, respectively.

Poly(*rac*-lactide)$_m$-*b*-poly(trimethylene glycol)$_n$-*b*-poly(*rac*-lactide)$_m$ (P*r*LA$_m$-*b*-PO3G$_n$-*b*-P*r*LA$_m$) copolymers were obtained using the same procedure using *rac*-lactide (a mixture 50:50 of *D*-:*L*-lactide) instead of *L*-Lactide and $PO3G_n$ macroinitiators having MW=500 and 1000 and 2400 g·mol^{-1}.

Some copolymers were recovered either as a white powder or as a viscous oil, depending on the length of the macroinitiator used or the enantiomeric composition of the lactide used in the synthesis.

Preparation of nanoparticles

Nanoparticles were prepared using the oil-in-water single emulsion technique with minor modifications. Specifically, 10 mg of the PLA_m-*b*-$PO3G_n$-*b*-PLA_m triblock copolymer were dissolved in 2 mL of DCM and the solution was added to 10 mL of 1% (w/w) PVA aqueous solution. The mixture was sonicated using a Hielscher Ultrasonic Processor UP200St (E=3,200 J, c=100, A=20%) to yield a homogeneous oil-in-water emulsion. This emulsion was immediately poured into 10 mL of the 0.3% w/w PVA solution, and the mixture was magnetically stirred in an open beaker at room temperature for 3 h. The nanoparticles formed during the gradual evaporation of DCM. For SEM analysis, nanoparticles were collected by centrifugation at 9,500 r.p.m. for 15 min and washed three times with distilled water to remove the PVA emulsifier.

Results and discussion

The synthetic route for the synthesis of PLA_m-*b*-$PO3G_n$-*b*-PLA_m triblock copolymers using $Sn(Oct)_2$ as catalyst is shown in Scheme 1. Three $PO3G_n$ macroinitiators were used differing in the molecular weights. For each macroinitiator three series of triblock copolymers containing *L*- or *rac*-lactide were obtained varying the $PO3G_n$/lactide ratios. The results of these syntheses including molar feed ratio, compositions and molecular weights for the whole library of copolymers are collected in Table 1. $PO3G_n$ macroinitiator displays two hydroxyl-end groups, which can trigger the ROP of cyclic esters, e.g., *L*/*rac*-lactide, when assisted by a suitable catalyst.

We selected $Sn(Oct)_2$ because this catalyst is approved by the FDA for use in food and medical applications and for its high activity in the synthesis of PLA.[17] The reaction took place in bulk at 180 °C and was easily followed by ^{1}H NMR as the methine signals from the lactide monomer (CH, 5.03 ppm) and polymer (CH, 5.17 ppm) appeared well-resolved (Figure 1a and Figure S1 of electronic supporting information (ESI)). By comparing both signals, it is possible to quantify the unreacted monomer. We first explored the evolution of the ROP of *L*-lactide initiated by $PO3G_{41}$ (M_n=2,400 g·mol^{-1}) (Figure 1b). A burst in the early stage of the ROP is observed, with 91% of *L*-lactide reacting after 30 min. Subsequently, the polymerization proceeded steadily until the equilibrium was reached and approximately 96% of the monomer was consumed in nearly 1.5 h. Three different concentrations of $Sn(Oct)_2$ catalyst were tested, and based on both the conversion over time results and the catalyst amount (Figure 1b), the intermediate concentration (0.05% by weight of lactide) was ultimately selected. The ROP of *L*-lactide proceeded satisfactorily in a relative short time; nonetheless, species other than the selected macroinitiator, i.e., water, can indeed interfere in the polymerization and parallelly compete for a site in the final polymer architecture. As we will show later, this side reaction was not observed during the synthesis of these copolymers, as the ratio of reacted macroinitiator end groups to triblock copolymer end groups was close to one.

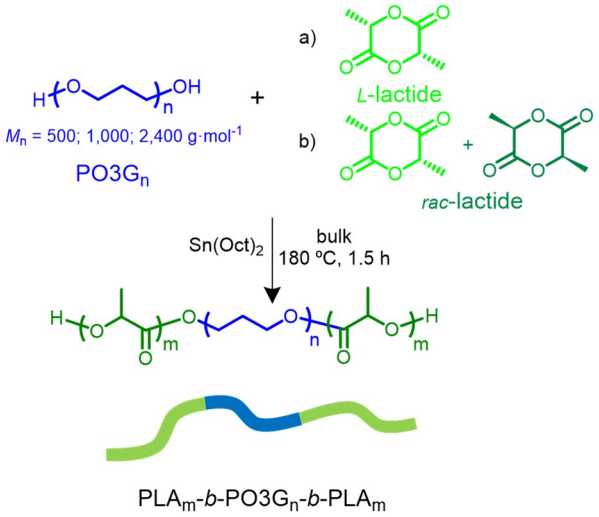

Scheme 1 Synthetic pathway for the preparation of bio-based poly(ether-ester)s triblock copolymers from $PO3G_n$ and a) *L*-lactide or b) *rac*-lactide.

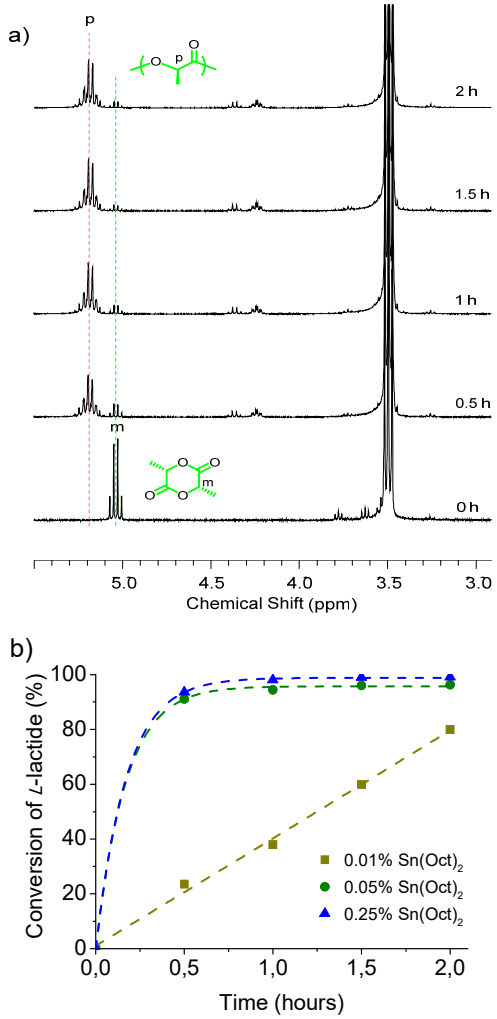

Figure 1 (a) ^{1}H-NMR ($CDCl_3$) spectra of the P*L*LA_{21}-*b*-$PO3G_{41}$-*b*-P*L*LA_{21} copolymer at different reaction times using 0.05% $Sn(Oct)_2$ catalyst and, (b) conversion of *L*-lactide in the ROP initiated by the $PO3G_{41}$ macroinitiator at different catalyst concentrations.

View Article Online
DOI: 10.1039/D5PY00594A

Table 1 ROP of *L*/*rac*-lactide initiated by $PO3G_n$ macroinitiator mediated by $Sn(Oct)_2$ catalyst (0.05% w/w).

Entry	Macroinitiator	Copolymer[a]	Feed[b]	Experimental[c]	SEC			
			$[PO3G_n]/[PLA]$	$[PO3G_n]/[PLA]$	M_n ($g\cdot mol^{-1}$)	M_n ($g\cdot mol^{-1}$)	M_w ($g\cdot mol^{-1}$)	$Đ$
1	$PO3G_9$				560	1,030	1,690	1.7
2		P*L*LA$_{4.5}$-*b*-$PO3G_9$-*b*-P*L*LA$_{4.5}$	50/50	56/44	1,030	1,680	2,260	1.4
3		P*L*LA$_9$-*b*-$PO3G_9$-*b*-P*L*LA$_9$	33/67	38/62	1,560	2,540	3,230	1.3
4		P*L*LA$_{18}$-*b*-$PO3G_9$-*b*-P*L*LA$_{18}$	20/80	22/78	2,730	4,630	5,510	1.2
5		P*r*LA$_{4.5}$-*b*-$PO3G_9$-*b*-P*r*LA$_{4.5}$	50/50	57/43	920	1,670	2,230	1.3
6		P*r*LA$_9$-*b*-$PO3G_9$-*b*-P*r*LA$_9$	33/67	38/62	1,650	2,510	3,130	1.3
7		P*r*LA$_{18}$-*b*-$PO3G_9$-*b*-P*r*LA$_{18}$	20/80	22/78	2,930	4,430	5,380	1.2
8	$PO3G_{17}$				1,140	1,690	3,530	2.1
9		P*L*LA$_{8.5}$-*b*-$PO3G_{17}$-*b*-P*L*LA$_{8.5}$	50/50	61/39	2,050	2,440	4,360	1.8
10		P*L*LA$_{17}$-*b*-$PO3G_{17}$-*b*-P*L*LA$_{17}$	25/75	39/61	3,900	5,530	6,805	1.2
11		P*L*LA$_{34}$-*b*-$PO3G_{17}$-*b*-P*L*LA$_{34}$	20/80	22/78	6,030	10,010	11,770	1.2
12		P*r*LA$_{8.5}$-*b*-$PO3G_{17}$-*b*-P*r*LA$_{8.5}$	50/50	58/42	2,290	3,740	5,280	1.4
13		P*r*LA$_{17}$-*b*-$PO3G_{17}$-*b*-P*r*LA$_{17}$	33/67	37/63	3,830	5,660	7,120	1.3
14		P*r*LA$_{34}$-*b*-$PO3G_{17}$-*b*-P*r*LA$_{34}$	20/80	22/78	5,230	7,760	9,510	1.2
15	$PO3G_{41}$				2,510	4,490	9,270	2.1
16		P*L*LA$_{21}$-*b*-$PO3G_{41}$-*b*-P*L*LA$_{21}$	50/50	59/41	3,920	7,880	11,150	1.4
17		P*L*LA$_{41}$-*b*-$PO3G_{41}$-*b*-P*L*LA$_{41}$	33/67	43/57	5,240	9,230	12,410	1.3
18		P*L*LA$_{82}$-*b*-$PO3G_{41}$-*b*-P*L*LA$_{82}$	20/80	23/77	11,710	19,030	23,080	1.2
19		P*r*LA$_{21}$-*b*-$PO3G_{41}$-*b*-P*r*LA$_{21}$	50/50	61/39	3,850	6,830	10,250	1.5
20		P*r*LA$_{41}$-*b*-$PO3G_{41}$-*b*-P*r*LA$_{41}$	33/67	45/55	5,070	7,760	11,050	1.4
21		P*r*LA$_{82}$-*b*-$PO3G_{41}$-*b*-P*r*LA$_{82}$	20/80	22/78	13,830	16,730	21,600	1.3

[a] Subscripts correspond to the degree of polymerization (DP) of each block used in the feed. [b] Molar feed ratio of $PO3G_n$ and PLA repeating units. [c] Experimental composition and M_n, calculated from OCH/OCH_2 signals and end groups analysis, respectively by ^1H NMR.

After purification, we took samples of the $PO3G_n$ macroinitiator and their block copolymers, to determine the molecular weights distributions (MWDs) by SEC analysis. Table 1 collects the SEC data for the macroinitiators and triblock copolymers. As expected, triblock copolymers displayed higher molecular weights than their respective macroinitiators, and increased with the content of lactide in the copolymers. The dispersity ($Đ$) of the $PO3G_n$ macroinitiators ranged from 1.7 to 2.1. On the other hand, in all series, $Đ$ was observed to decrease as the molecular weight or the content of lactide units in the copolymer increased. $Đ$ of 1.2-1.3 were obtained for the copolymers with higher content of lactide. Monomodal and narrow MWDs were obtained, indicating excellent control over the polymerization (Figure 2). The results suggest that $Sn(Oct)_2$ serves as an efficient catalyst for the ROP of lactide, initiated by the macroinitiator, with significantly reduced interchain transesterification. Thus, SEC traces provided evidence that the -OH end groups in $PO3G_n$ were the sole species that initiated the ROP of lactide. The constitution and composition of the copoly(ether-ester)s were ascertained by ^1H and ^{13}C NMR spectroscopy, which clearly discriminates between methylene and methine protons from $PO3G_n$ and *L*-lactide units, respectively. As an example, Figure 3 shows representative NMR spectra recorded for the P*L*LA$_{82}$-*b*-$PO3G_{41}$-*b*-P*L*LA$_{82}$ copolymer. Compositions were determined by integration of the CH signal of lactide units (signal c) and the first methylene protons of $PO3G_n$ units (signal e). The composition for all series were close to those of $PO3G_n$ and *L*-lactide used in the feed and exhibit acceptable consistency, with small deviations due to partial volatilization of lactide during ROP. On the other hand, the signal corresponding to the methylene protons of $PO3G_n$ attached to the first lactide unit (signal d), which appeared as a multiplet, showed an integral twice that of the C*H*OH end groups (signal b). This further

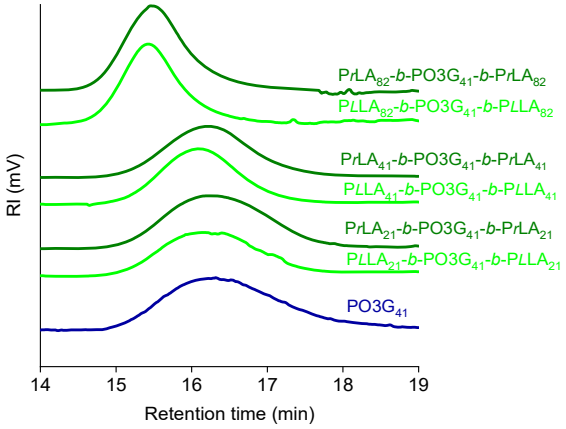

Figure 2 SEC traces of $PO3G_{41}$ macroinitiator and the PLA_m-*b*-$PO3G_{41}$-*b*-PLA_m triblock copolymers.

View Article Online
DOI: 10.1039/D5PY00594A

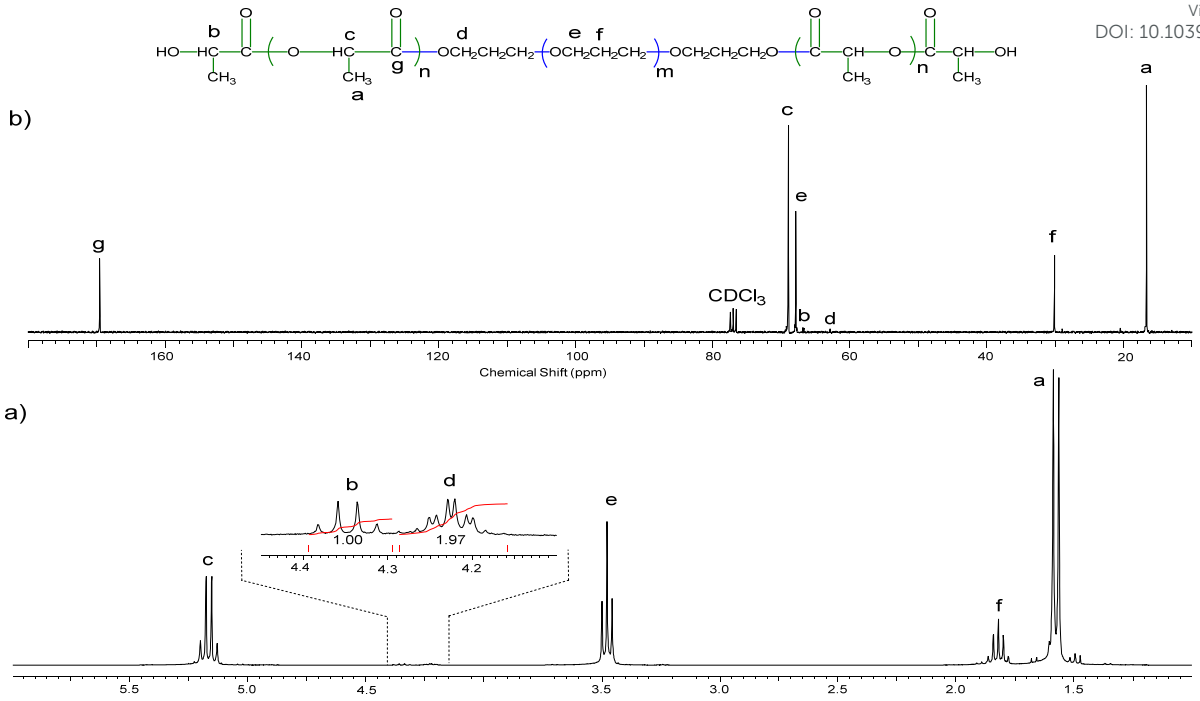

Figure 3 (a)^{1}H- and (b) ^{13}C-NMR spectrum in $CDCl_3$ of P*L*LA$_{82}$-*b*-PO3G$_{41}$-P*L*LA$_{82}$ copolymer

confirmed the triblock structure of the copolymers and the absence of any PLA chains initiated by other species, such as water. Spectra recorded for P*r*LA$_{82}$-*b*-PO3G$_{41}$-*b*-P*r*LA$_{82}$ and two selected P*L*LA$_m$-*b*-PO3G$_{41}$-*b*-P*L*LA$_m$ and P*r*LA$_m$-*b*-PO3G$_{41}$-*b*-P*r*LA$_m$ series can be found in Figures S2-S6 of the ESI. The spectra of triblock copolymers obtained using *rac*-lactide instead of *L*-lactide showed broader signals in the ^{1}H NMR and splitting in the ^{13}C NMR peaks due to the presence of different stereosequences in the PLA blocks (Figure S2).[26]

In addition, FT-IR further corroborated the chemical structure of the obtained copolymers (Figure 4). The infrared spectrum of PO3G$_{41}$ displayed a strong absorption band at 1,102 cm^{-1}, corresponding to the C–O–C asymmetric stretching vibration of the ether groups. The incorporation of lactide units at the end groups of PO3G$_n$ to form the triblock copolymer was confirmed by the presence of the C=O carbonyl band at 1,751 cm^{-1} and the C(=O)–O stretching band at 1,181 cm^{-1}, which are characteristics of the ester groups of the lactide units. These absorptions increased in intensity as the lactide content increased in the P*L*LA$_m$-*b*-PO3G$_{41}$-*b*-P*L*LA$_m$ copolymer series. Furthermore, signals attributed to CH_2 stretching (2,859 cm^{-1}) decreased, while those related to CH_3 bending (1,453 cm^{-1}) increased, as the copolymer was enriched in lactide units.

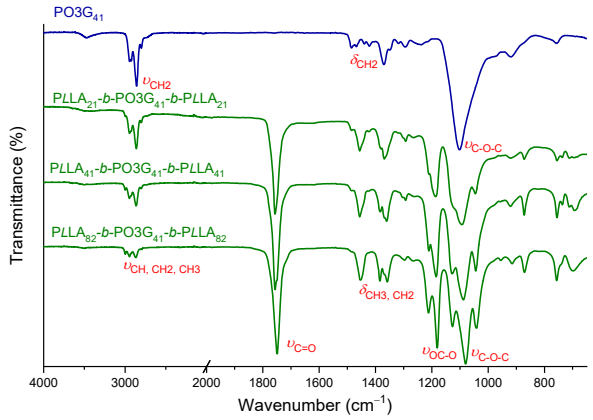

Figure 4 FT-IR spectra of PO3G$_{41}$ macroinitiator and P*L*LA$_m$-*b*-PO3G$_{41}$-*b*-P*L*LA$_m$ triblock copolymers.

Thermal properties of triblock copolymers

To investigate the thermal stability and transitions of these copolymers, TGA and DSC analyses were performed. The data collected by these analyses for each series of PLA$_m$-*b*-PO3G$_n$-*b*-PLA$_m$ triblock copolymers, as well as for the PO3G$_n$ macroinitiators, are displayed in Table 2. The TGA traces recorded for the PLA$_m$-*b*-PO3G$_{41}$-*b*-PLA$_m$ series and their derivatives curves are shown in Figure 5. For the rest of the series, both TGA traces and derivatives curves are accessible in Figures S7 and S8 of the ESI File. The onset temperature ($^{o}T_d$) of PO3G$_{41}$ decreased in the copolymers as polylactide blocks were incorporated at its ends; in contrast, the derivative curve splits into two main events: the maximum decomposition rate ($^{max}T_d$) exhibited two maxima at temperatures close to their parent polymers: the former found in the 273-289 °C range, that was ascribed to the degradation of PLA blocks, and the latter ranging from 408-428 °C, attributed to the degradation of the more thermally stable PO3G$_{41}$ block. It is noteworthy to highlight that there was no more than 1% residue left at temperatures far from 450 °C, and in several cases, there was no residue at all.

View Article Online
DOI: 10.1039/D5PY00594A

Table 2 Thermal properties of the PLA_m-*b*-$PO3G_n$-*b*-PLA_m triblock copolymers.

Polymer		TGA [a]				DSC [b]						
						Cooling			Second heating			
		$^{\circ}T_d$ (°C)	$^{max}T_d$ (°C)	R_w (%)	[PO3G]/[PLA]	T_g (°C)	T_c (°C)	ΔH_c (J·g^{-1})	T_{cc} (°C)	ΔH_{cc} (J·g^{-1})	T_m (°C)	ΔH_m (J·g^{-1})
$PO3G_9$		248	398	0	100/0	-82	-	-	-40	-60	10	70
	$PLLA_{4.5}$-*b*-$PO3G_9$-*b*-$PLLA_{4.5}$	247	282/410	1	42/58	-41	-	-	-	-	-	-
	$PLLA_9$-*b*-$PO3G_9$-*b*-$PLLA_9$	250	281/408	0	25/75	-11	-	-	-	-	-	-
	$PLLA_{18}$-*b*-$PO3G_9$-*b*-$PLLA_{18}$	246	273/391	1	13/87	15	-	-	80	-9	107	13
	$PrLA_{4.5}$-*b*-$PO3G_9$-*b*-$PrLA_{4.5}$	261	282/404	1	45/55	-43	-	-	-	-	-	-
	$PrLA_9$-*b*-$PO3G_9$-*b*-$PrLA_9$	273	301/401	1	25/75	-17	-	-	-	-	-	-
	$PrLA_{18}$-*b*-$PO3G_9$-*b*-$PrLA_{18}$	260	289/395	1	14/86	8	-	-	-	-	-	-
$PO3G_{17}$		335	410	1	100/0	-77	-	-	-40	-64	13	93
	$PLLA_{8.5}$-*b*-$PO3G_{17}$-*b*-$PLLA_{8.5}$	246	269/425	1	49/51	-44	-	-	-	-	-	-
	$PLLA_{17}$-*b*-$PO3G_{17}$-*b*-$PLLA_{17}$	238	286/417	0	32/68	-6	-	-	33/68	-11/-15	100	15
	$PLLA_{34}$-*b*-$PO3G_{17}$-*b*-$PLLA_{34}$	247	270/411	0	18/82	26	94	-36	-	-	144	38
	$PrLA_{8.5}$-*b*-$PO3G_{17}$-*b*-$PrLA_{8.5}$	242	266/424	1	49/51	-41	-	-	-	-	-	-
	$PrLA_{17}$-*b*-$PO3G_{17}$-*b*-$PrLA_{17}$	246	268/407	2	31/69	-13	-	-	-	-	-	-
	$PrLA_{34}$-*b*-$PO3G_{17}$-*b*-$PrLA_{34}$	246	268/407	1	19/81	12	-	-	-	-	-	-
$PO3G_{41}$		306	381	0	100/0	-75	-	-	-40	-57	17	80
	$PLLA_{21}$-*b*-$PO3G_{41}$-*b*-$PLLA_{21}$	261	273/428	0	51/49	-33	57/23	-7/-2	65	-3	100	4
	$PLLA_{41}$-*b*-$PO3G_{41}$-*b*-$PLLA_{41}$	272	289/428	0	37/63	-14	77	-26	-	-	126	26
	$PLLA_{82}$-*b*-$PO3G_{41}$-*b*-$PLLA_{82}$	252	275/408	0	18/82	32	95	-36	-	-	156	41
	$PrLA_{21}$-*b*-$PO3G_{41}$-*b*-$PrLA_{21}$	241	254/428	0	54/46	-49	-	-	-	-	-	-
	$PrLA_{41}$-*b*-$PO3G_{41}$-*b*-$PrLA_{41}$	251	286/408	1	38/62	-16	-	-	-	-	-	-
	$PrLA_{82}$-*b*-$PO3G_{41}$-*b*-$PrLA_{82}$	260	315/412	1	18/82	26	-	-	-	-	-	-
$PLLA_{68}$		255	338	0	100/0	47	101	-40	88	-10	152	47
$PrLA_{68}$		287	354	0	100/0	43	-	-	-	-	-	-

[a] Onset temperature for 10% of weight loss ($^{\circ}T_d$), maximum rate ($^{max}T_d$) decomposition temperatures and remaining weight (R_w) and weight-% composition ([PO3G]/[PLA]) after heating at 600 °C. [b] Glass transition (T_g), crystallization (T_c and ΔH_c) and melting (T_m and ΔH_m) temperatures and enthalpies measured by DSC.

Minor differences in the thermal analysis were observed for the PLA_m-*b*-$PO3G_9$-*b*-PLA_m and PLA_m-*b*-$PO3G_{17}$-*b*-PLA_m series, with deviations hardly surpassing 10% in some cases (Figures S7 and S8 of the ESI). The TGA analysis, additionally, provided valuable information on the chemical constitution. Since the derivative curve exhibited two well-defined and resolved decomposition steps, the composition of each copolymer could be ascertained by integration of these curves. Figure 5b, for instance, displays the derivative curve of the P*L*LA_{21}-*b*-$PO3G_{41}$-*b*-P*L*LA_{21} copolymer: the areas under each curve reveal direct composition by weight of the copolymers. The

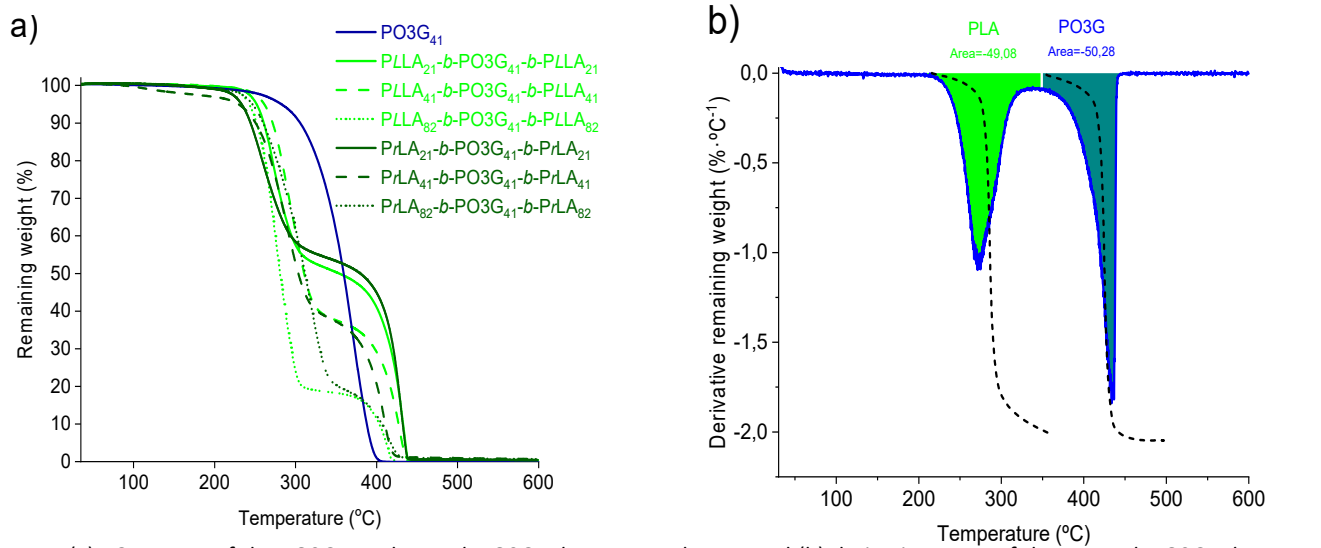

Figure 5 (a) TGA traces of the $PO3G_{41}$ and PLA_m-*b*-$PO3G_{41}$-*b*-PLA_m copolymers and (b) derivative curve of the P*L*LA_{21}-*b*-$PO3G_{41}$-*b*-P*L*LA_{21} copolymer

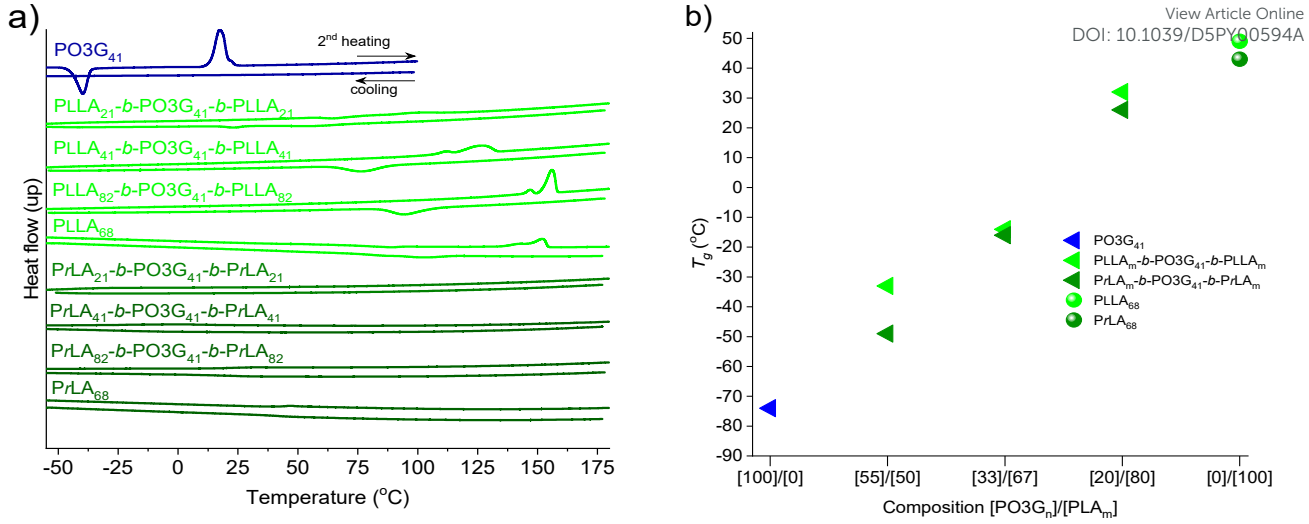

Figure 6 (a) DSC second heating and cooling traces of the PLA_m-*b*-$PO3G_{41}$-*b*-PLA_m triblock copolymers, and (b) T_g *vs* molar composition of PLA_m-*b*-$PO3G_{41}$-*b*-PLA_m copolymers.

extracted values for each series (Table 2) are close with small variations to those obtained by ^{1}H NMR (Table 1). To explore the influence of copolymer composition on crystallinity and melting temperatures, DSC was used to investigate their thermal behavior. In Figure 6a, we present a comparative view of the recorded DSC traces from cooling scans and second heating for the P*L*LA_m-*b*-$PO3G_{41}$-*b*-P*L*LA_m and P*r*LA_m-*b*-$PO3G_{41}$-*b*-P*r*LA_m copolymer series as well as their parent macroinitiator. $PO3G_{41}$ displays an endothermic peak at 17 °C due to the melting process of the macroinitiator crystalline domains after a cold crystallization process that was observed to happen at -40 °C. On all copolymer series, no peak due to melting or crystallization of the inner macroinitiator was observed. This phenomenon can be attributed to the PLA segments attached to the end $PO3G_n$ end groups that restrict the chain mobility. [27, 28] On the other hand, there was a clear trend in the melting process attributed to the PLA segments, situated in the 95-155 °C range. As the composition or the length of the *L*-lactide blocks in the copolymers increase, the melting temperature shifts to that of the one observed for its parent homopolymer, i.e., P*L*LA_{68}. This shift toward higher temperatures, approaching to the melting point of P*L*LA, is directly correlated with the degree of polymerization (DP) of the lactide blocks. In other words, as the DP of the PLA segments increases, the melting temperature of the copolymers also rises. This behavior can be attributed to an increase in lamellar thickness, as longer chains are capable of forming more stable and thicker crystalline lamellae. When the copolymers are cooled from the melt, a crystallization event appears and follows a similar trend as the copolymer composition changes. As it was expected, P*r*LA_m-*b*-$PO3G_{41}$-*b*-P*r*LA_m copolymers did not exhibit any (endo/exo) thermic peak. Similar behavior was observed for the PLA_m-*b*-$PO3G_{9}/_{34}$-*b*-PLA_m copolymers, whose thermograms are accessible in Figures S9-S11 of the ESI file.

All of the copolymers exhibited a single, second-order glass transition temperature (T_g), which increased almost linearly with the lactide content in all the series of copolymers studied. Figure 6b shows the T_g versus composition for the PLA_m-*b*-$PO3G_{41}$-*b*-PLA_m series. As illustrated, the copolymer T_g values fall between –49 °C and 32 °C, intermediate to those of $PO3G_{41}$ and PLA_{68} homopolymers (Figure S12), confirming the full miscibility between the PLA and $PO3G_n$ blocks.[10, 29]

Self-assembling in aqueous media

In the search for innovative nanomaterials, we explored the ability of the PLA_m-*b*-$PO3G_n$-*b*-PLA_m amphiphilic triblock copolymers to self-assemble in water. We used the well-established emulsion-evaporation method for obtaining the nanoparticles due to the good solubility of copolymers in DCM,[30, 31] enabling the fabrication of a library of nanomaterials. As representative examples, Table 3 collects sizes, polydispersity indexes (PDI's) and zeta potentials (ζ) acquired by DLS measurements for the PLA_m-*b*-$PO3G_{41}$-*b*-PLA_m copolymer series. Unimodal distributions evidenced the occurrence of a self-assembling event, while Ẕ-average diameters oscillating between 95 and 171 nm and narrow PDI's, confirmed the presence of nanometric aggregates (Figure 7a-c). The correlation coefficients, whose values were close to 1 (inset in DLS profiles), strengthened the reliability and

Table 3 Ẕ-average diameter (nm), PDI and zeta potential (ζ) of the nanoparticles obtained from PLA_m-*b*-$PO3G_{41}$-*b*-PLA_m triblock copolymers.

Copolymer	Size (nm)	PDI	ζ (mV)
P*L*LA_{21}-*b*-$PO3G_{41}$-*b*-P*L*LA_{21}	171	0.09	-5
P*L*LA_{41}-*b*-$PO3G_{41}$-*b*-P*L*LA_{41}	170	0.08	-9
P*L*LA_{82}-*b*-$PO3G_{41}$-*b*-P*L*LA_{82}	124	0.12	-4
P*r*LA_{21}-*b*-$PO3G_{41}$-*b*-P*r*LA_{21}	104	0.17	-10
P*r*LA_{41}-*b*-$PO3G_{41}$-*b*-P*r*LA_{41}	95	0.24	-8
P*r*LA_{82}-*b*-$PO3G_{41}$-*b*-P*r*LA_{82}	109	0.13	-9

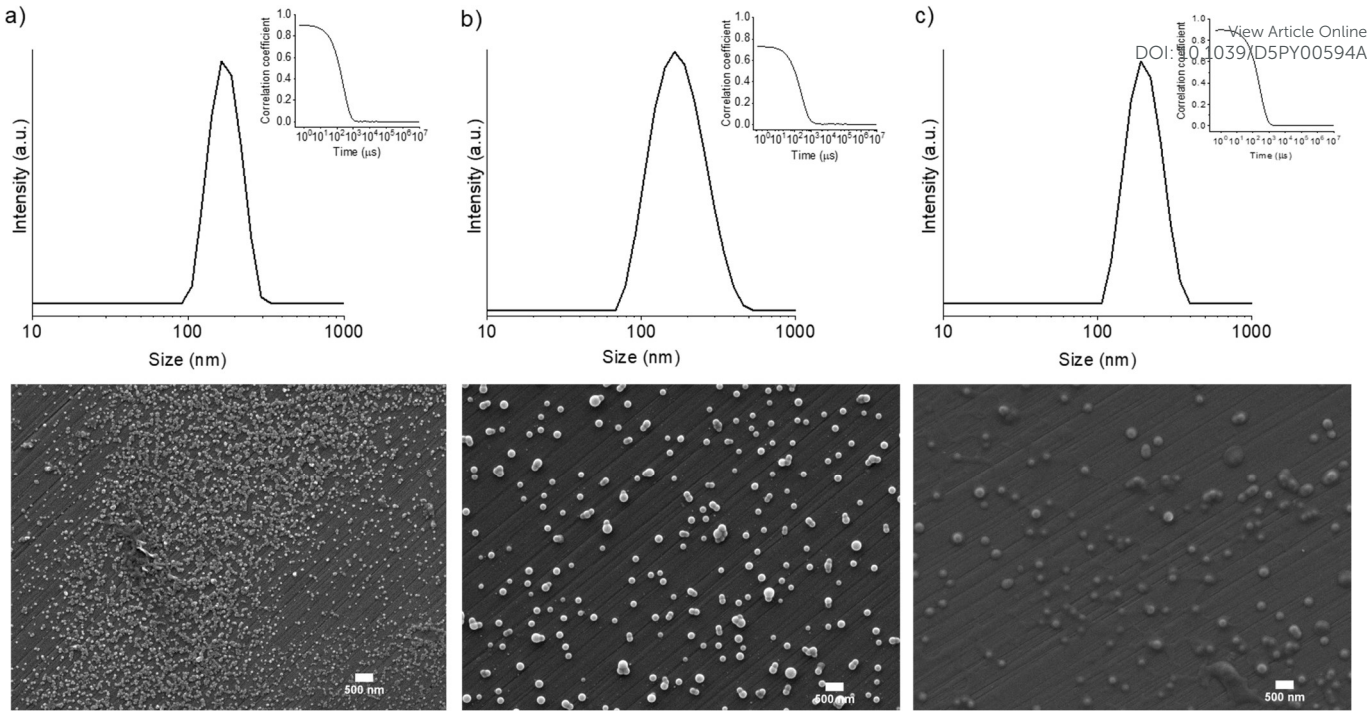

Figure 7 (Top) DLS profiles (inset: correlation coefficient) and (bottom) SEM images of (a) P*r*LA$_{82}$-*b*-PO3G$_{41}$-*b*-P*r*LA$_{82}$ (b) P*r*LA$_{41}$-*b*-PO3G$_{41}$-*b*-P*r*LA$_{41}$ and (c) P*L*LA$_{21}$-*b*-PO3G$_{41}$-b-P*L*LA$_{21}$ triblock copolymers. Scale bar = 500 nm.

quality of the DLS data. Interestingly, NPs from P*r*LA$_m$-*b*-PO3G$_{41}$-*b*-P*r*LA$_m$ copolymers displayed smaller sizes than P*L*LA$_m$-b-PO3G$_{41}$-*b*-P*L*LAm, a fact that could be a direct consequence of the amorphous or semicrystalline structure adopted by the hydrophobic core in the nanoparticle. The amorphous PLA blocks can pack more efficiently than semicrystalline blocks in core of the nanoparticle allowing the nanoparticle self-assemble with reduced dimensions. [32] DSC scans of two types of selected nanoparticles revealed two key observations (Figure S13 of ESI). First, the T_g of the self-assembled nanoparticles were found to be 23 and 26 °C higher than that of the corresponding bulk materials. This suggests that during the self-assembly process, the PLA and PO$_3$Gn blocks rearrange according to their affinity for water, forming a core–shell nanostructure with well-defined nanoscale phase segregation. Second, the T_g of nanoparticles derived from *rac*-lactide showed enthalpic relaxation phenomena, indicating efficient packing and compaction of the amorphous chains. In all cases, nanoparticles displayed negative zeta potentials, with values hardly distant between them across the entire series. DLS data for the PLA$_m$-*b*-PO3G$_9$/$_{17}$-*b*-PLA$_m$ series can be found in Table S1 of the ESI file. Ƶ-average diameters between 102 and 158 nm and negative z-potentials ranging from -4 to -20 were obtained for the PLA$_m$-*b*-PO3G$_9$-*b*-PLA$_m$ copolymers. The PLA$_m$-*b*-PO3G$_{17}$-*b*-PLA$_m$ exhibited ƶ-average diameters of 115-144 nm with negative z-potentials in the -2 to -20 range. To further comprehend the adopted morphology of these nanoaggregates, SEM shed light on their shape. Illustrative images from selected copolymers are shown in Figure 7, bottom. To our delight, we observed well-delineated-spherical nanoobjects, which sizes matched in good consistency to those obtained by DLS.

Conclusions

A bio-based polyol derived from 1,3-propanediol was employed to prepare triblock copoly(ether-ester)s. The two hydroxyl end groups of the PO3G$_n$ polyol serve as efficient initiators for the ROP of *L*-lactide or *rac*-lactide. Using solventless ROP, we generated a library of BAB-type copolymers with predictable degrees of polymerization, whose compositions were readily tuned by varying the [PO3G]/[lactide] feed ratio. Thermal analysis showed these copolymers to be stable up to approximately 250 °C, undergoing decomposition in a two-step process. Crystallinity could be adjusted by selecting the lactide stereochemistry and tailoring the triblock composition. Since PLA and PO3G$_n$ segments are fully miscible, the glass transition temperature (T_g) of the entire series can be modulated simply by altering the [PO3G]/[lactide] ratio, enabling precise control over material properties. These novel, fully bio-based polymers exhibit *pseudo*-amphiphilic behaviour in aqueous solution. As a proof-of-concept, dynamic light scattering (DLS) and scanning electron microscopy (SEM) confirmed that the poly(ether-ester) copolymers self-assembled into nanometric particles in water. We anticipate that this protocol will pave the way for designing innovative nanodevices that could be used for biomedical applications *via* ROP of different cyclic esters using PO3G$_n$ as macroinitiator.

Author contributions

A. M. de I. conceived the idea and proposed the strategy. E. T. D. and E. C. Z. and A. M. de I. designed the experiments, carry out the

experimental work, evaluated the data, and wrote the manuscript together. All participated in data analysis. All the authors proofread the manuscript.

Conflicts of interest

There are no conflicts to declare.

Data availability

All data supporting the findings of this study are available within the article and its ESI.† Raw experimental data are available from the corresponding author upon reasonable request.

Acknowledgements

We want to thank the Ministerio de Ciencia, Innovación y Universidades of Spain (MCIU/AEI/FEDER, UE) (Project RTI2018-095041-B-C33) and the Technological University of Catalonia (UPC) (AGRUPS R-02520) for their financial support. The authors would also like to acknowledge Dr. Judit Canadell (TotalEnergies-Corbion) for the *L*- and *rac*-lactide monomers and Dr. Peter Talbiersky from Allessa for the $PO3G_n$ samples kindly provided for this study. E. T. D. acknowledges the postdoctoral grant Margarita Salas awarded in 2021 by Spanish government.

Notes and references

(1) Rosenboom, J.-G.; Langer, R.; Traverso, G. Bioplastics for a circular economy. *Nature Reviews Materials* **2022**, *7* (2), 117-137. DOI: 10.1038/s41578-021-00407-8.

(2) von Vacano, B.; Mangold, H.; Vandermeulen, G. W. M.; Battagliarin, G.; Hofmann, M.; Bean, J.; Künkel, A. Sustainable Design of Structural and Functional Polymers for a Circular Economy. *Angewandte Chemie International Edition* **2023**, *62* (12), e202210823. DOI: https://doi.org/10.1002/anie.202210823.

(3) Sardon, H.; Mecerreyes, D.; Basterretxea, A.; Avérous, L.; Jehanno, C. From Lab to Market: Current Strategies for the Production of Biobased Polyols. *ACS Sustainable Chemistry & Engineering* **2021**, *9* (32), 10664-10677. DOI: 10.1021/acssuschemeng.1c02361.

(4) Harmer, M. A.; Confer, D. C.; Hoffman, C. K.; Jackson, S. C.; Liauw, A. Y.; Minter, A. R.; Murphy, E. R.; Spence, R. E.; Sunkara, H. B. Renewably sourced polytrimethylene ether glycol by superacid catalyzed condensation of 1,3-propanediol. *Green Chemistry* **2010**, *12* (8), 1410-1416, 10.1039/C002443K. DOI: 10.1039/c002443k.

(5) Lee, H.-N.; Rosen, B. M.; Fenyvesi, G.; Sunkara, H. B. UCST and LCST phase behavior of poly(trimethylene ether) glycol in water. *Journal of Polymer Science Part A: Polymer Chemistry* **2012**, *50* (20), 4311-4315. DOI: https://doi.org/10.1002/pola.26242.

(6) Delavarde, A.; Savin, G.; Derkenne, P.; Boursier, M.; Morales-Cerrada, R.; Nottelet, B.; Pinaud, J.; Caillol, S. Sustainable polyurethanes: toward new cutting-edge opportunities. *Progress in Polymer Science* **2024**, *151*, 101805. DOI: https://doi.org/10.1016/j.progpolymsci.2024.101805.

(7) Li, Y.; Liu, Y.; Liu, A.; Xu, C.; Zhang, C.; Yu, J.; Yuan, R.; Li, F. Poly(trimethylene terephthalate-b-poly(trimethylene ether) glycol) copolymers: From bio-based thermoplastic elastomers to elastic fibers for apparel. *European Polymer Journal* **2025**, *225*, 113706. DOI: https://doi.org/10.1016/j.eurpolymj.2024.113706.

(8) Jiang, J.; Tang, Q.; Pan, X.; Xi, Z.; Zhao, L.; Yuan, W. Structure and Morphology of Thermoplastic Polyamide Elastomer Based on Long-Chain Polyamide 1212 and Renewable Poly(trimethylene glycol). *Industrial & Engineering Chemistry Research* **2020**, *59* (39), 17502-17512. DOI: 10.1021/acs.iecr.0c01334.

(9) Kasprzyk, P.; Głowińska, E.; Parcheta-Szwindowska, P.; Rohde, K.; Datta, J. Green TPUs from Prepolymer Mixtures Designed by Controlling the Chemical Structure of Flexible Segments. In *International Journal of Molecular Sciences*, 2021; Vol. 22.

(10) Petchsuk, A.; Klinsukhon, W.; Sirikittikul, D.; Prahsarn, C. Parameters affecting transition temperatures of poly(lactic acid-co-polydiols) copolymer-based polyester urethanes and their shape memory behavior. *Polymers for Advanced Technologies* **2012**, *23* (8), 1166-1173. DOI: https://doi.org/10.1002/pat.2017.

(11) Ugarte, L.; Saralegi, A.; Fernández, R.; Martín, L.; Corcuera, M. A.; Eceiza, A. Flexible polyurethane foams based on 100% renewably sourced polyols. *Industrial Crops and Products* **2014**, *62*, 545-551. DOI: https://doi.org/10.1016/j.indcrop.2014.09.028.

(12) Jung, Y.-S.; Lee, S.; Park, J.; Shin, E.-J. One-Shot Synthesis of Thermoplastic Polyurethane Based on Bio-Polyol (Polytrimethylene Ether Glycol) and Characterization of Micro-Phase Separation. *Polymers* **2022**, *14* (20), 4269.

(13) Wang, H.; Wang, Y.; Yuan, C.; Xu, X.; Zhou, W.; Huang, Y.; Lu, H.; Zheng, Y.; Luo, G.; Shang, J.; et al. Polyethylene glycol (PEG)-associated immune responses triggered by clinically relevant lipid nanoparticles in rats. *npj Vaccines* **2023**, *8* (1), 169. DOI: 10.1038/s41541-023-00766-z.

(14) Kozma, G. T.; Shimizu, T.; Ishida, T.; Szebeni, J. Anti-PEG antibodies: Properties, formation, testing and role in adverse immune reactions to PEGylated nano-biopharmaceuticals. *Advanced Drug Delivery Reviews* **2020**, *154-155*, 163-175. DOI: https://doi.org/10.1016/j.addr.2020.07.024.

(15) Zhang, Y.; Zhang, A. Y.; Feng, Z. G.; Ye, L.; Xu, R. X. Synthesis and characterization of polyether esters elastomer based on polyethylene glycol and poly(butylene terephthalate) - Influence of different hard segment length on polymer properties. *Acta Polymerica Sinica* **2002**, (2), 167-172.

(16) Khouri, N. G.; Bahú, J. O.; Blanco-Llamero, C.; Severino, P.; Concha, V. O. C.; Souto, E. B. Polylactic acid (PLA): Properties, synthesis, and biomedical applications – A review of the literature. *Journal of Molecular Structure* **2024**, *1309*, 138243. DOI: https://doi.org/10.1016/j.molstruc.2024.138243.

(17) Masutani, K.; Kimura, Y.; Chemistry, R. S. o. PLA Synthesis. From the Monomer to the Polymer. In *Poly(lactic acid) Science and Technology: Processing, Properties, Additives and Applications*, Jiménez, A., Peltzer, M., Ruseckaite, R. Eds.; The Royal Society of Chemistry, 2014; p 0.

(18) Murariu, M.; Dubois, P. PLA composites: From production to properties. *Advanced Drug Delivery Reviews* **2016**, *107*, 17-46. DOI: https://doi.org/10.1016/j.addr.2016.04.003.

(19) Saeidlou, S.; Huneault, M. A.; Li, H.; Park, C. B. Poly(lactic acid) crystallization. *Progress in Polymer Science* **2012**, *37* (12), 1657-1677. DOI: https://doi.org/10.1016/j.progpolymsci.2012.07.005.

(20) Müller, A. J.; Ávila, M.; Saenz, G.; Salazar, J.; Chemistry, R. S. o. Crystallization of PLA-based Materials. In *Poly(lactic acid) Science and Technology: Processing, Properties, Additives and Applications*, Jiménez, A., Peltzer, M., Ruseckaite, R. Eds.; The Royal Society of Chemistry, 2014; p 0.

(21) De Luca, S.; Milanese, D.; Gallichi-Nottiani, D.; Cavazza, A.; Sciancalepore, C. Poly(lactic acid) and Its Blends for Packaging Application: A Review. In *Clean Technologies*, 2023; Vol. 5, pp 1304-1343.

(22) Swetha, T. A.; Bora, A.; Mohanrasu, K.; Balaji, P.; Raja, R.; Ponnuchamy, K.; Muthusamy, G.; Arun, A. A comprehensive review on polylactic acid (PLA) – Synthesis, processing and application in food packaging. *International Journal of Biological Macromolecules* **2023**, *234*, 123715. DOI: https://doi.org/10.1016/j.ijbiomac.2023.123715.

(23) da Silva, D.; Kaduri, M.; Poley, M.; Adir, O.; Krinsky, N.; Shainsky-Roitman, J.; Schroeder, A. Biocompatibility, biodegradation and excretion of polylactic acid (PLA) in medical implants and theranostic systems. *Chem Eng J* **2018**, *340*, 9-14. DOI: 10.1016/j.cej.2018.01.010 From NLM.

(24) Suk, J. S.; Xu, Q.; Kim, N.; Hanes, J.; Ensign, L. M. PEGylation as a strategy for improving nanoparticle-based drug and gene delivery. *Advanced Drug Delivery Reviews* **2016**, *99*, 28-51. DOI: https://doi.org/10.1016/j.addr.2015.09.012.

(25) Shi, D.; Beasock, D.; Fessler, A.; Szebeni, J.; Ljubimova, J. Y.; Afonin, K. A.; Dobrovolskaia, M. A. To PEGylate or not to PEGylate: Immunological properties of nanomedicine's most popular component, polyethylene glycol and its alternatives. *Advanced Drug Delivery Reviews* **2022**, *180*, 114079. DOI: https://doi.org/10.1016/j.addr.2021.114079.

(26) Thakur, K. A. M.; Kean, R. T.; Hall, E. S.; Kolstad, J. J.; Lindgren, T. A.; Doscotch, M. A.; Siepmann, J. I.; Munson, E. J. High-Resolution 13C and 1H Solution NMR Study of Poly(lactide). *Macromolecules* **1997**, *30* (8), 2422-2428. DOI: 10.1021/ma9615967.

(27) Ding, Y.; Feng, W.; Lu, B.; Wang, P.; Wang, G.; Ji, J. PLA-PEG-PLA tri-block copolymers: Effective compatibilizers for promotion of the interfacial structure and mechanical properties of PLA/PBAT blends. *Polymer* **2018**, *146*, 179-187. DOI: https://doi.org/10.1016/j.polymer.2018.05.037.

(28) Bao, J.; Dong, X.; Chen, S.; Lu, W.; Zhang, X.; Chen, W. Confined crystallization, melting behavior and morphology in PEG-b-PLA diblock copolymers: Amorphous versus crystalline PLA. *Journal of Polymer Science* **2020**, *58* (3), 455-465. DOI: https://doi.org/10.1002/pol.20190077.

(29) Olabisi, O.; Robeson, L. M. S. M. T. *Polymer-polymer miscibility*; Academic Press, 1979.

(30) Staff, R. H.; Landfester, K.; Crespy, D. Recent Advances in the Emulsion Solvent Evaporation Technique for the Preparation of Nanoparticles and Nanocapsules. In *Hierarchical Macromolecular Structures: 60 Years after the Staudinger Nobel Prize II*, Percec, V. Ed.; Springer International Publishing, 2013; pp 329-344.

(31) Tinajero-Díaz, E.; Martínez de Ilarduya, A.; Muñoz-Guerra, S. Synthesis and properties of diblock copolymers of ω-pentadecalactone and α-amino acids. *European Polymer Journal* **2019**, *116*, 169-179. DOI: https://doi.org/10.1016/j.eurpolymj.2019.04.009.

(32) Panyam, J.; Labhasetwar, V. Biodegradable nanoparticles for drug and gene delivery to cells and tissue. *Advanced Drug Delivery Reviews* **2003**, *55* (3), 329-347. DOI: https://doi.org/10.1016/S0169-409X(02)00228-4.

View Article Online
DOI: 10.1039/D5PY00594A

Data availability

All data supporting the findings of this study are available within the article and its ESI.† Raw experimental data are available from the corresponding author upon reasonable request.